Geosci. Model Dev. Discuss., https://doi.org/10.5194/gmd-2018-21
Manuscript under review for journal Geosci. Model Dev.
Discussion started: 29 March 2018

Geoscientific Model Development Discussions

Adaptive Cartesian Meshes for Atmospheric Single-Column Models, a study using Basilisk 18-02-16

J.Antoon van Hooft[1], Stéphane Popinet[2], and Bas J.H. van de Wiel[1]

[1]Delft University of Technology, Department of Geoscience and Remote Sensing, Delft, The Netherlands
[2]Sorbonne Universités, UPMC Univ Paris 06, CNRS, UMR 7190, Institut Jean Le Rond d'Alembert, Paris, France

Correspondence to: Antoon van Hooft (j.a.vanhooft@tudelft.nl)

Abstract. It is well known that the representation of certain atmospheric conditions in climate and weather models can still suffer from the limited grid resolution that is facilitated by modern-day computer systems. Herein we study a simple one-dimensional analogy to those models by using a Single-Column Model (SCM) description of the atmosphere. The model employs an adaptive Cartesian mesh that applies a high-resolution mesh only when and where it is required. The so-called adaptive-grid model is described and we report on our findings obtained for tests to evaluate the representation of the atmospheric boundary layer, based on the first two GABLS intercomparison cases. The analysis shows that the adaptive-grid algorithm is able to dynamically coarsen and refine the numerical grid whilst maintaining an accurate solution. This is an interesting result as in reality, transitional dynamics (e.g. due to the diurnal cycle or due to changing synoptic conditions) are rule rather than exception.

1 Introduction

Single-Column Models (SCMs) are often used as the building blocks for Global (or General) Circulation Models (GCMs). As such, many of the lessons learned from SCM development can be inherited by GCMs and hence the evaluations of SCMs receives considerable attention by the geoscientific model development community (see e.g. Neggers et al., 2012; Bosveld et al., 2014; Baas et al., 2017). In this work, we present a SCM that employs an adaptive Cartesian mesh that can drastically reduce the computational costs of such models, especially when pushing the model's resolution. The philosophy is inspired by recently obtained results on the evolution of atmospheric turbulence in a daytime boundary layer using three dimensional (3D) adaptive grids. As promising results were obtained for turbulence resolving techniques such as Direct Numerical Simulations and Large-eddy Simulation (LES), herein we explore whether similar advancements can be made with more practically oriented techniques for the numerical modelling of the atmosphere. As such, the present model uses Reynolds-averaged Navier-Stokes techniques (Reynolds, 1895) to parameterize the vertical mixing processes due to turbulence, as is typical in weather and climate models.

Geosci. Model Dev. Discuss., https://doi.org/10.5194/gmd-2018-21
Manuscript under review for journal Geosci. Model Dev.
Discussion started: 29 March 2018

Geoscientific Model Development Discussions

The discussion of limited grid resolution is present in many studies of SCMs and GCMs. A prominent example is the nocturnal cumulus-cloud case (Wyant et al., 2007): whereas a high resolution mesh is required for capturing the processes at the cloud interface, a coarser resolution may be used for the time when the sun has risen and the cloud has been dissolved. More generally speaking, virtually all of the atmospheric dynamics that require a relatively high-resolution grid for their representation in numerical models are localized in both space and in time. The issue is made more difficult to tackle by the fact that their spatio-temporal localization is typically not known a priori (e.g. the height and strength of a future inversion layer). Therefore, the pre-tuned and static-type grids that most operational GCMs use (virtually all) are not flexible enough to capture all dynamical regimes accurately or efficiently. This also puts a large strain on the used closures for the sub-grid scale processes. In order to mitigate this challenge, GCMs that employ a so-called adaptive grid have been explored in the literature. Here the grid resolution adaptively varies in both space and time, focussing the computational resources to where and when they are most necessary. Most notably, the innovative works of Jablonowski (2004), Jablonowski et al. (2009) and St-Cyr et al. (2008) report on the usage of both Cartesian and non-conforming three-dimensional adaptive grids and clearly demonstrate the potential of grid adaptivity for GCMs. Inspired by their works, we follow a 1D SCM approach and aim to add to their findings, using different grid-adaptative formulations and solver strategies. Since SCMs do not resolve large-scale atmospheric circulations, the analysis herein focusses on the representation of the Atmospheric Boundary Layer (ABL).

Over the years, the computational resources that are available to run computer models have increased considerably (Schaller, 1997). This has facilitated GCMs to increase their models' spatial resolution. However, it is important to realize that for virtually all physical processes, the (spatial and temporal) fraction of the domain that actually calls for the increasing maximum resolution decreases. By definition, with an increasing resolved scale separation, only an adaptive-grid approach is able to reflect the effective (or fractal) dimension of the physical system in the scaling of the computational costs (Popinet, 2011; Van Hooft et al., 2018). This is an important aspect where the present adaptive-grid approach differs from for example, a dynamic-grid approach (see e.g. Dunbar et al., 2008), that employs a fixed number of grid cells that needs to be predefined by the user. This work departs from the method for grid adaptation as presented in the work of Van Hooft et al. (2018) on 3D-turbulence-resolving simulations of the ABL. As such, this work is also based on the adaptive-grid toolbox and build-in solvers provided by the 'Basilisk' code (http://basilisk.fr).

We test our model with the well established cases defined for the first two GABLS intercomparison projects for SCMs. As part of the Global Energy and Water cycle EXchanges (GEWEX) modelling and prediction panel, the GEWEX ABL Study (GABLS) was initiated in 2001 to improve understanding of the atmospheric boundary layer processes and their representation in models. Based on observations during field campaigns, a variety of model cases has been designed and studied using both LES and SCMs with a large set of models using traditional static-grid structures. An overview of the results and their interpretation for the first three intercomparison cases are presented in the work of Holtslag et al. (2013). Here we will test the present adaptive-grid SCM based on the first two intercomparison cases, referred to as GABLS1 and GABLS2. These cases were designed to study the model representation of the stable boundary layer and the diurnal cycle, respectively. Their scenarios prescribe idealized atmospheric conditions and lack the complete set of physical processes and interactions encountered in reality. At this stage within our research, the authors consider this aspect to be an advantage, as the present SCM model does

Geosci. Model Dev. Discuss., https://doi.org/10.5194/gmd-2018-21
Manuscript under review for journal Geosci. Model Dev.
Discussion started: 29 March 2018

Geoscientific Model Development Discussions
Open Access
EGU

not have a complete set of parametrizations for all processes that are typically found in the operational models (see e.g. Slingo, 1987; Grell et al., 2005)).

This paper is organized as follows, the present SCM is discussed in more detail in Sect. 2. The results based on the first two GABLS intercomparison scenarios are presented in Sect. 3. Finally, a discussion and conclusions are presented in Sect. 4. Furthermore, in the Appendix A, a validation of the used solver formulation is given for a simplified flow problem (i.e. the laminar Ekman spiral).

2 Model Overview

As we focus on the merits of grid adaptivity in this study on SCMs and not on the state-of-the-art closures for the vertical transport phenomena, we have opted to employ simple and well-known descriptions for the turbulent transport processes. More specifically, the present model uses a stability-dependent, first-order, local, K-diffusivity closure as presented in the seminal works of Louis (1982) and Beljaars et al. (1989). For the surface-flux parametrizations we again follow the work of Louis (1982). The used closures are not repeated here but are summarized in section 2 of Holtslag and Boville (1993). However, to improve the representation of mixing under stable conditions, an alteration is made to the formulation of the so-called stability-correction function ($F(\mathrm{Ri})$) under stably-stratified conditions. Based on the work of England and McNider (1995), we use a so-called short-tail mixing function,

$$F(\mathrm{Ri}) = \begin{cases} 0, & \mathrm{Ri} \geq 0.2, \\ \left(1 - \frac{\mathrm{Ri}}{0.2}\right)^2, & 0 \leq \mathrm{Ri} < 0.2, \\ \text{Louis et al. (1982)}, & \mathrm{Ri} < 0, \end{cases} \tag{1}$$

where Ri is the local and bulk Richardson number for the evaluation of turbulent diffusivities and the surface transport, respectively. The authors of this work realize that there has been considerable advancements on the representation of mixing under unstable conditions in the past decades, e.g non-local mixing (Holtslag and Boville, 1993) and turbulent-kinetic-energy-based closures (see e.g., Mellor and Yamada, 1982; Lenderink and Holtslag, 2004). Therefore, we would like to note that such schemes are compatible with the adaptive-grid approach and they could be readily employed to improve the physical descriptions in the present model. From an implementations' perspective those schemes would not require any grid-adaptation specific considerations when using the Basilisk code.

The most prominent feature of the SCM presented in this work is its ability to dynamically coarsen and refine the grid resolution based on the evolution of the solution itself. As mentioned in the introduction, the associated grid-adaptation algorithm is the same as was used by Van Hooft et al. (2018). We only briefly discuss the general concept here. For an in-depth quantitative discussion with an example, the reader is referred to the aforementioned paper.

Apart from the imperfect representation of the physical aspects of a system in numerical models, additional errors naturally arise due to the spatial and temporal discretization. In general, a higher resolution corresponds to a more accurate solution and a simulation result is considered to be 'converged' when the numerically obtained solution and its statistics of interest do not

Geosci. Model Dev. Discuss., https://doi.org/10.5194/gmd-2018-21
Manuscript under review for journal Geosci. Model Dev.
Discussion started: 29 March 2018

Geoscientific Model Development Discussions

crucially depend on the chosen resolution. The aim of the grid-adaptation algorithm is to dynamically coarsen and refine the mesh so that the errors due to the spatial discretization remain within limited bounds and to be *uniformly distributed* in both space and time. For our adaptive approach this requires, (1) an algorithm that evaluates a local estimate of the discretization error in the representation of selected solution fields and (2), a corresponding error threshold (ζ) that determines if a grid cell's resolution is either too fine, too coarse or just fine. Grid adaptation can then be carried out accordingly. The 'error estimator' is based on a so-called multi-resolution analysis that is formally linked to wavelet thresholding. The error threshold, or so-called refinement criterion ζ, is defined by the user. Noting that similar to the pre-tuning of the fixed-in-time grids as is common in most SCMs, the grid resolution remains at the discretion of the model's user.

In this work we base the refinement and coarsening of the grid on a second-order-accurate estimated discretization error in the solution fields for the horizontal wind components ($\boldsymbol{u} = (u, v)$) and the virtual potential temperature (θ_v). Based on trail and error, we set the corresponding refinement criteria,

$$\zeta_{u,v} = 0.25 \text{ m/s}, \tag{2}$$

$$\zeta_{\theta_v} = 0.5 \text{ K}, \tag{3}$$

for both of the horizontal wind components and virtual potential temperature, respectively. In practice, the grid-adaptation algorithm strongly relates the resolved local 'curvature' of the solution fields to the local grid resolution, where high curvature corresponds to a high resolution. The tree-based anisotropic-grid structure in Basilisk facilitates a convenient basis for the multi-resolution analysis and the subsequent refinement and coarsening of cells at integer levels of refinement. This entails that the spatial resolution can vary by factors of two (Popinet, 2011).

For time integration; we recognize a reaction-diffusion-type equation describing the evolution of the horizontal wind components and scalar fields such as the virtual potential temperature and specific humidity (q_t). For a variable field $s(z,t)$, we write,

$$\frac{\partial s}{\partial t} = \nabla \cdot (K \nabla s) + r. \tag{4}$$

Where r is a source term and K is the diffusion coefficient. Using a time-implicit first-order-accurate time discretization with timestep Δt separating the solution s^n and s^{n+1}, this can be written,

$$\frac{s^{n+1} - s^n}{\Delta t} = \nabla \cdot (K \nabla s^{n+1}) + r. \tag{5}$$

Rearranging the terms we get,

$$\nabla \cdot (K \nabla s^{n+1}) - \frac{s^{n+1}}{\Delta t} = -\frac{s^n}{\Delta t} - r. \tag{6}$$

To obtain a Poisson-Helmholtz equation, that is solved for using a multigrid strategy, employing a finite-volume-type second-order-accurate spatial discretization (Popinet, 2017a, b). The physical timestep is adaptively varied between 2 sec. and 15 sec. based on the convergence properties of the aforementioned iterative solver. Noting that these values are rather small compared

Geosci. Model Dev. Discuss., https://doi.org/10.5194/gmd-2018-21
Manuscript under review for journal Geosci. Model Dev.
Discussion started: 29 March 2018

Geoscientific Model Development Discussions
Open Access
EGU

to existing SCMs that often employ higher-order-accurate time-integration schemes. The solver's second-order spatial accuracy is validated and its performance scaling is accessed for a simple flow set-up in Appendix A. For the exact details of the model set-ups for the cases presented in this paper, the reader is referred to the case-definition files (in legible formatting). Links are provided to their online locations in table 1.

3 Results

3.1 GABLS1

The first GABLS intercomparison case focusses on the representation of a stable boundary layer. Its scenario was inspired by the LES study of an ABL over the Arctic sea by Kosović and Curry (2000). The results from the participating SCMs are summarized and discussed in Cuxart et al. (2006), for the LES intercomparison study, the reader is referred to the work of Beare et al. (2006). The case prescribes the initial profiles for wind and temperature, a constant geostrophic forcing of $U_{geo} = 8$ m/s and a fixed surface-cooling rate of 0.25 K/hour. The model is set-up accordingly, with a maximum resolution of 6.25 meter, corresponding to 6 levels of refinement and a domain height of 400 meters.

Due to the idealizations in the case set-up with respect to the reality of the field observations, the model results were not compared against the experimental data (Cuxart et al., 2006). However, for the SCMs, a reference was found in the high-fidelity LES results that tended to agree well between the various models. The LES results therefore serve as a benchmark for the results obtained with the present model. This facilitates a straight forward testing of the formulations and implementations of the used physical closures, before we continue our analysis towards the full diurnal cycle. Inspired by the analysis of Cuxart et al. (2006) and *their* figure 3, we compare our SCM results with the 6.25 meter-resolution LES ensemble results. We focus on the profiles for the wind components and potential temperature averaged over the eighth hour of the simulation in Fig. 1. We observe that the present SCM is in good agreement with the LES results and is able to capture the vertical structure of the ABL, including the low-level jet. The differences are only minor compared to the variations in the results presented in the aforementioned GABLS1 SCM reference paper.

Noting that in general, results are of course sensitive to the closure chosen to parametrize the turbulent transport, in our case given by Eq.1. In order to separate between the numerical effects of using grid adaptivity and the chosen physical closures, we define an additional reference case in which we run an *equidistant-grid* SCM. This model run employs a fixed 6.25 meter resolution (i.e with 64 cells), but otherwise identical closures and numerical formulations. I.e. we have switched-off the grid adaptivity and maintain the maximum resolution throughout the domain. We can observe that results between both SCMs are in good agreement but, that minor deviations are present. These discrepancies are in the order of magnitude of the refinement criteria and can be reduced by choosing more stringent values (see Appendix A), that would result in using more grid cells. The evolution of the adaptive-grid structure is shown in Fig. 2 a. We see that a relatively high resolution is employed near the surface, i.e. in the logarithmic layer. Remarkably, without any a priori knowledge, the grid is refined at a height of $150\ \mathrm{m} < z < 200\ \mathrm{m}$ as the so-called low-level jet develops, whereas the grid has remained coarse above the boundary layer where the grid resolution

Geosci. Model Dev. Discuss., https://doi.org/10.5194/gmd-2018-21
Manuscript under review for journal Geosci. Model Dev.
Discussion started: 29 March 2018

Geoscientific Model Development Discussions

was reduced to be as coarse as 100 meters. From Fig.2 b we learn that the number of grid cells varied between 11 and 22 over the course of the simulation run.

3.2 GABLS2

The second GABLS model intercomparison case was designed to study the model representation of the ABL over the course of two consecutive diurnal cycles. The case is set-up after the observations that were collected on the 22th and 23rd of October, 1999 during the CASES-99 field experiment in Leon, Kansas, USA (Poulos et al., 2002). The details are described (and not repeated here) in the work of Svensson et al. (2011) that was dedicated to the evaluation of the SCM results for the GABLS2 intercomparison. Compared to the original case prescriptions, we choose a slightly higher domain size of $z_{top} = 4096$ meters (compared to 4000 m), so that a maximum resolution of 8 meters corresponds to 9 levels of refinement.

In this section we place our model output in the context of the results presented in the work of Svensson et al. (2011), that, apart from the SCM results, also includes the results from the LES by Kumar et al. (2010). To obtain their data we have used the so-called 'data digitizer' of Rohatgi (2018). Inspired by the analysis of Svensson et al. (2011) and *their* figures 10 and 11, we intercompare our results for the wind-speed magnitude ($U = \|\boldsymbol{u}\|$) and virtual potential temperature profiles in Fig. 3 a and b, respectively. Here we see that the results obtained with the present SCM fall within the range of the results as were found with the selected models that participated in the original intercomparison. These models also employed a first-order-style turbulence closure and have a lowest model-level height of less than 5 meters. Fig. 3 c presents a timeseries of the 10-meter wind speed (U_{10m}) during the 22-th of October. Again the present model results compare well with the others. Next, in order to validate the grid-adaptivity independently from the used closures, we present the hourly evolution of the wind speed on the 23-rd of October against the results obtained with adaptivity switched off, using 512 *equally-spaced* grid points in Fig. 4. We clearly see that the evolution of the wind speed profile is the same and even the small-scale features in the inversion layer (i.e. $z \approx 800$ m) are present in the adaptive-grid model calculations. The corresponding evolution of the adaptive-grid structure is presented in Fig. 2, where the colours in the resolution plot appear to sketch a 'Stullian' image (see figure 1.7 in the book of Stull, 1988). Apparently, the grid-adaptation algorithm has identified (!) the 'surface layer' within the convective boundary layer, the stable boundary layer, the entrainment zone and the inversion layer as the dynamic regions that require a high-resolution mesh. The total number of grid cells varied between 24 and 44.

4 Discussion & Conclusions

In this work we have presented an one-dimensional (1D) single-column model (SCM) that employs a mesh whose resolution is varied adaptively based on the evolution of the numerically obtained solution. This is an attractive feature because it is a prerequisite to enable the computational effort required for the evaluation of numerical solution to scale with the complexity of the studied physical system. The adaptation algorithm based on limiting discretization errors appears to function very well for a wide variety of geophysical applications: e.g. 3D atmospheric turbulence-resolving models (Van Hooft et al., 2018), tsunami and ocean-wave modelling (Popinet, 2011; Beetham et al., 2016; Marivela-Colmenarejo, 2017), hydrology (Kirstetter et al.,

2016), two-phase micro physics (Howland et al., 2016), flow of granular media (Zhou et al., 2017) and shock-wave formation (Eggers et al., 2017). For these studies on highly dynamical systems, the adaptive-grid approach is chosen because it offers a more computationally effcient approach as compared to the usage of static grids.

The present work does not include an assessment and discussion on the performance of the presented methods in relation to the computational speed. Even though this is an important motivation for the application of the adaptive-grid strategy to GCMs, the authors argue that an SCM is not suitable for speed-performance testing: the speed of single-column calculations is virtually never a critical issue. Only in 3D mode, when SCMs are 'stitched together' to enable the resolving of global circulations, the model's computational efficiency becomes an issue. Furthermore, the performance of a SCM that employs a few tens of cells is not a good indicator for the performance of a GCM that can employ billions of grid cells. For the latter, parallel computation overhead and the so-called memory bottle neck are important aspects. Whereas for the SCM case, the complete instruction set and solution data can typically be loaded onto the cache memory of a single CPU's core. Nevertheless, for the readers' reference, the required run times for the different SCM set-ups presented herein are listed in table 1, and figure A1b in Appendix A also presents quantitative results on this topic and shows that the adaptive-grid solver is well behaved.

Following the turbulence resolving study of Van Hooft et al. (2018), the results presented herein are a proof-of-concept for future 3D modelling, using RANS techniques. The authors of this work realize that the present SCM is a far cry from a complete global model and that more research and development is required before the method can be compared on a global-circulation scale. As shown by e.g. Jablonowski (2004), a 3D adaptive grid also allows a variable grid resolution in the horizontal directions. This further enables the computational resources to focus on the most challenging atmospheric processes where there is a time and spatial variation in the horizontal-resolution requirement of the grid. Examples include the contrasting dynamics between relatively calm centres of high-pressure circulations and those characterizing stormy low-pressure cells. Also, in the case of a sea breeze event (Arrillaga et al., 2018), it would be beneficial to temporarily increase the horizontal resolution near the land–sea interface. As such, we encourage the usage of this technique for those meteorologically challenging scenarios.

Acknowledgements. The authors gratefully acknowledge the funding by the ERC Consolidator grant (648666). The LES ensemble results used for the GABLS1 intercomparison are kindly made available by Bob Beare; online via: http://gabls.metoffice.com/.

Competing interests. The authors declare that there are no competing interests.

Code and data availability. Basilisk is a freely available (GPLv3), multi-purpose tool to solve partial differential equations and has it's own website: http://www.basilisk.fr. The code contains solvers for Saint-Venant problems, the Navier-Stokes equations, electrohydrodynamics and more, see http://basilisk.fr/src/README. A selection of examples can be viewed online: http://www.basilisk.fr/src/examples. The website also provides general information including; installation instructions and a tutorial. Furthermore, for the work herein, interested readers can visit the model set-up pages and links to their online locations are presented in table 1. The data can easily be generated by

Geosci. Model Dev. Discuss., https://doi.org/10.5194/gmd-2018-21
Manuscript under review for journal Geosci. Model Dev.
Discussion started: 29 March 2018

Geoscientific Model Development Discussions

running the scripts. Finally, a snapshot of the used code, as it was used in this the work, is made available via ZENODO, with doi link: https://doi.org/10.5281/zenodo.1203631.

Appendix A: The Ekman Spiral

In this Appendix we validate the numerical solver by evaluating its convergence characteristics for a one dimensional (1D) Ekman-flow set-up. We test both the equidistant-grid and the adaptive-grid approaches. The case describes a neutrally-stratified fluid with kinematic viscosity ν and density ρ in a rotating frame of reference with angular velocity Ω. A flow is forced by a horizontal pressure gradient $\mathrm{d}P/\mathrm{d}y = U_{geo} f \rho$, over a no-slip bottom boundary (located at $z_{bottom} = 0$). Where U_{geo} is a velocity scale that is also known as the geostrophic wind. There exists an analytical, 1D, steady solution for the horizontal wind components (u_E, v_E), that is known as the Ekman spiral;

$$u_E = U_{geo}\left(1 - e^{-\gamma z}\cos(\gamma z)\right), \tag{A1}$$

$$v_E = U_{geo} e^{-\gamma z}\sin(\gamma z), \tag{A2}$$

with γ the so-called Ekman depth, $\gamma = \sqrt{\Omega/\nu}$. We initialize our model and set boundary conditions consistent with Eqs A1 and A2. Using a domain height of $L = 100\gamma$. The error (η) in the numerically obtained solution (u^n, v^n) is evaluated as,

$$\eta = \int_{z_{bottom}}^{z_{top}} \|u^n - u_E\| + \|v^n - v_E\| \mathrm{d}z, \tag{A3}$$

at the end of the run that is performed until $t_{end} = 10 \times \gamma/U_{geo}$, with a timestep $\Delta t = 0.01 \times \gamma/U_{geo}$. We study the spatial-convergence properties of the fixed-grid solver and the adaptive-grid approach by iteratively decreasing the (maximum) grid size. For the adaptive-grid solver we decrease the refinement criteria ζ for the velocity components accordingly[1]. In order to facilate a comparison between the methods, we diagnose the used cells for the adaptive grid run. Figure A1 a shows that both approaches are second-order accurate. Were the adaptive grid results are more accurate than the results from the fixed-grid approach, employing the same number of grid cells. Figure A1 b shows that for both approaches the required effort (i.e. in wall-clock time) scales linearly with the number of grid cells, except for the runs that require less than one-tenth of a second to perform. This plots reveals that *per grid cell* there is computational overhead for the adaptive-grid approach. The results in this appendix show that the used numerical methods are well behaved.

[1]The details of the exact case set-up can be found online: www.basilisk.fr/sandbox/Antoonvh/ekmanfg.c

Geosci. Model Dev. Discuss., https://doi.org/10.5194/gmd-2018-21
Manuscript under review for journal Geosci. Model Dev.
Discussion started: 29 March 2018

References

Arrillaga, J., Vilà-Guerau de Arellano, J., Bosveld, F., Klein Baltink, H., Yagüe, C., Sastre, M., and Román-Cascón, C.: Impacts of afternoon and evening sea-breeze fronts on local turbulence and CO2 and 222Rn transport, Quart. J. Roy. Meteor. Soc. (under review), 2018.

Baas, P., van de Wiel, B., van der Linden, S., and Bosveld, F.: From Near-Neutral to Strongly Stratified: Adequately Modelling the Clear-Sky Nocturnal Boundary Layer at Cabauw, Boundary-Layer Meteorology, pp. 1–22, 2017.

Beare, R. J., Macvean, M. K., Holtslag, A. A., Cuxart, J., Esau, I., Golaz, J.-C., Jimenez, M. A., Khairoutdinov, M., Kosovic, B., Lewellen, D., et al.: An intercomparison of large-eddy simulations of the stable boundary layer, Boundary-Layer Meteorology, 118, 247–272, 2006.

Beetham, E., Kench, P. S., O'Callaghan, J., and Popinet, S.: Wave transformation and shoreline water level on Funafuti Atoll, Tuvalu, Journal of Geophysical Research: Oceans, 121, 311–326, 2016.

Beljaars, A. C. M., Holtslag, A., and Van Westrhenen, R.: Description of a software library for the calculation of surface fluxes, KNMI De Bilt, Netherlands, 1989.

Bosveld, F. C., Baas, P., Steeneveld, G.-J., Holtslag, A. A., Angevine, W. M., Bazile, E., de Bruijn, E. I., Deacu, D., Edwards, J. M., Ek, M., et al.: The third GABLS intercomparison case for evaluation studies of boundary-layer models. Part B: results and process understanding, Boundary-layer meteorology, 152, 157–187, 2014.

Cuxart, J., Holtslag, A. A., Beare, R. J., Bazile, E., Beljaars, A., Cheng, A., Conangla, L., Ek, M., Freedman, F., Hamdi, R., et al.: Single-column model intercomparison for a stably stratified atmospheric boundary layer, Boundary-Layer Meteorology, 118, 273–303, 2006.

Dunbar, T., Hanert, E., and Hogan, R.: A one-dimensional finite-element boundary-layer model with a vertical adaptive grid, Boundary-layer meteorology, 128, 459–472, 2008.

Eggers, J., Grava, T., Herrada, M., and Pitton, G.: Spatial structure of shock formation, Journal of Fluid Mechanics, 820, 208–231, 2017.

England, D. E. and McNider, R. T.: Stability functions based upon shear functions, Boundary-Layer Meteorology, 74, 113–130, 1995.

Grell, G. A., Peckham, S. E., Schmitz, R., McKeen, S. A., Frost, G., Skamarock, W. C., and Eder, B.: Fully coupled "online" chemistry within the WRF model, Atmospheric Environment, 39, 6957–6975, 2005.

Holtslag, A. and Boville, B.: Local versus nonlocal boundary-layer diffusion in a global climate model, Journal of Climate, 6, 1825–1842, 1993.

Holtslag, A., Svensson, G., Baas, P., Basu, S., Beare, B., Beljaars, A., Bosveld, F., Cuxart, J., Lindvall, J., Steeneveld, G., et al.: Stable atmospheric boundary layers and diurnal cycles: challenges for weather and climate models, Bulletin of the American Meteorological Society, 94, 1691–1706, 2013.

Howland, C. J., Antkowiak, A., Castrejón-Pita, J. R., Howison, S. D., Oliver, J. M., Style, R. W., and Castrejón-Pita, A. A.: It's Harder to Splash on Soft Solids, Physical review letters, 117, 184 502, 2016.

Jablonowski, C.: Adaptive grids in weather and climate modeling, Ph.D. thesis, University of Michigan, 2004.

Jablonowski, C., Oehmke, R. C., and Stout, Q. F.: Block-structured adaptive meshes and reduced grids for atmospheric general circulation models, Philosophical Transactions of the Royal Society of London A: Mathematical, Physical and Engineering Sciences, 367, 4497–4522, 2009.

Kirstetter, G., Hu, J., Delestre, O., Darboux, F., Lagrée, P.-Y., Popinet, S., Fullana, J.-M., and Josserand, C.: Modeling rain-driven overland flow: Empirical versus analytical friction terms in the shallow water approximation, Journal of Hydrology, 536, 1–9, 2016.

Kosović, B. and Curry, J. A.: A large eddy simulation study of a quasi-steady, stably stratified atmospheric boundary layer, Journal of the atmospheric sciences, 57, 1052–1068, 2000.

Kumar, V., Svensson, G., Holtslag, A., Meneveau, C., and Parlange, M. B.: Impact of surface flux formulations and geostrophic forcing on large-eddy simulations of diurnal atmospheric boundary layer flow, Journal of Applied Meteorology and Climatology, 49, 1496–1516, 2010.

Lenderink, G. and Holtslag, A. A.: An updated length-scale formulation for turbulent mixing in clear and cloudy boundary layers, Quarterly Journal of the Royal Meteorological Society, 130, 3405–3427, 2004.

Louis, J.: A short history of PBL parameterization at ECMWF, in: paper presented at the Workshop on Planetary Boundary Layer Parameterization, Eur. Cent. For Medium-Range Weather Forecasts, Reading, England, 1982, 1982.

Marivela-Colmenarejo, R.: Numerical Perspective on Tsunami Hazards and Their Mitigation by Coastal Vegetation, Ph.D. thesis, Virginia Tech, 2017.

Mellor, G. L. and Yamada, T.: Development of a turbulence closure model for geophysical fluid problems, Reviews of Geophysics, 20, 851–875, 1982.

Neggers, R. A., Siebesma, A. P., and Heus, T.: Continuous single-column model evaluation at a permanent meteorological supersite, Bulletin of the American Meteorological Society, 93, 1389–1400, 2012.

Popinet, S.: Quadtree-adaptive tsunami modelling, Ocean Dynamics, 61, 1261–1285, 2011.

Popinet, S.: Time-implicit discretisation of reaction–diffusion equations, http://www.basilisk.fr/src/diffusion.h, accessed: 2018-01-01, 2017a.

Popinet, S.: Multigrid Poisson-Helmholtz solvers, http://www.basilisk.fr/src/poisson.h, accessed: 2018-01-01, 2017b.

Poulos, G. S., Blumen, W., Fritts, D. C., Lundquist, J. K., Sun, J., Burns, S. P., Nappo, C., Banta, R., Newsom, R., Cuxart, J., et al.: CASES-99: A comprehensive investigation of the stable nocturnal boundary layer, Bulletin of the American Meteorological Society, 83, 555–581, 2002.

Reynolds, O.: On the dynamical theory of incompressible viscous fluids and the determination of the criterion., Philosophical transacations of the Royal Society of London, 56, 40–45, 1895.

Rohatgi, A.: WebPlotDigitizer, https://github.com/ankitrohatgi/WebPlotDigitizer, accessed via the web interface: 2018-01-01, 2018.

Schaller, R. R.: Moore's law: past, present and future, IEEE spectrum, 34, 52–59, 1997.

Slingo, J.: The development and verification of a cloud prediction scheme for the ECMWF model, Quarterly Journal of the Royal Meteorological Society, 113, 899–927, 1987.

St-Cyr, A., Jablonowski, C., Dennis, J. M., Tufo, H. M., and Thomas, S. J.: A comparison of two shallow-water models with nonconforming adaptive grids, Monthly Weather Review, 136, 1898–1922, 2008.

Stull, R. B.: An introduction to boundary layer meteorology, vol. 1, Springer Science & Business Media, 670 pp, 1988.

Svensson, G., Holtslag, A., Kumar, V., Mauritsen, T., Steeneveld, G., Angevine, W., Bazile, E., Beljaars, A., De Bruijn, E., Cheng, A., et al.: Evaluation of the diurnal cycle in the atmospheric boundary layer over land as represented by a variety of single-column models: the second GABLS experiment, Boundary-Layer Meteorology, 140, 177–206, 2011.

Van Hooft, J. A., Popinet, S., Van Heerwaarden, C. C., Van der Linden, S. J. A., de Roode, S. R., and Van de Wiel, B. J. H.: Towards Adaptive Grids for Atmospheric Boundary Layer Simulations, Boundary-Layer Meteorology, 999, 999–999, 2018.

Wyant, M. C., Bretherton, C. S., Chlond, A., Griffin, B. M., Kitagawa, H., Lappen, C.-L., Larson, V. E., Lock, A., Park, S., De Roode, S. R., et al.: A single-column model intercomparison of a heavily drizzling stratocumulus-topped boundary layer, Journal of Geophysical Research: Atmospheres, 112, 2007.

Zhou, Y., Lagrée, P.-Y., Popinet, S., Ruyer, P., and Aussillous, P.: Experiments on, and discrete and continuum simulations of, the discharge of granular media from silos with a lateral orifice, Journal of Fluid Mechanics, 829, 459–485, 2017.

Geosci. Model Dev. Discuss., https://doi.org/10.5194/gmd-2018-21
Manuscript under review for journal Geosci. Model Dev.
Discussion started: 29 March 2018

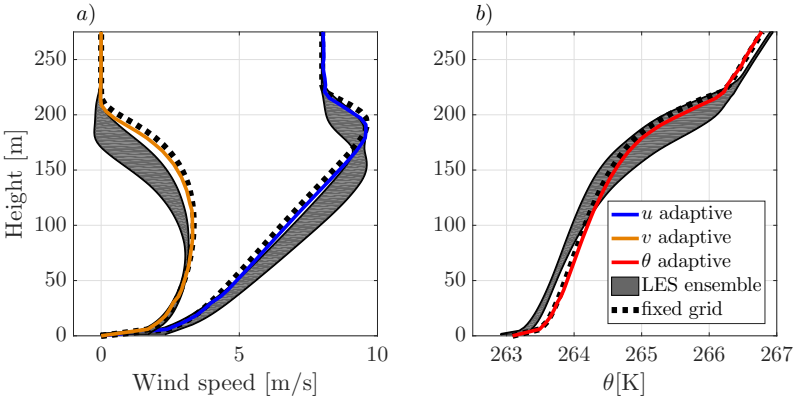

Figure 1. Time averaged profiles over the eight hour of the run according to the GABLS1 intercomparison scenario. For (a) the horizontal wind components and (b) the potential temperature. Results are obtained with the present adaptive-grid SCM (coloured lines), the LES models ensemble (i.e $\mathrm{mean} \pm \sigma$) from Beare et al. (2006) (grey-shaded areas) and the present SCM, employing an equidistant and static grid with a 6.25 meter resolution (dashed lines).

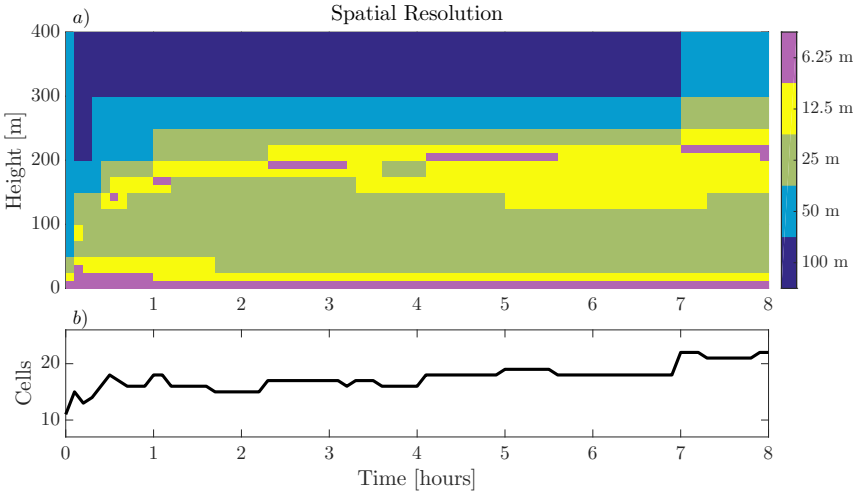

Figure 2. Evolution of (a) the vertical spatial-resolution distribution and (b) the total number of grid cells, for the GABLS1 intercomparison case.

Geosci. Model Dev. Discuss., https://doi.org/10.5194/gmd-2018-21
Manuscript under review for journal Geosci. Model Dev.
Discussion started: 29 March 2018

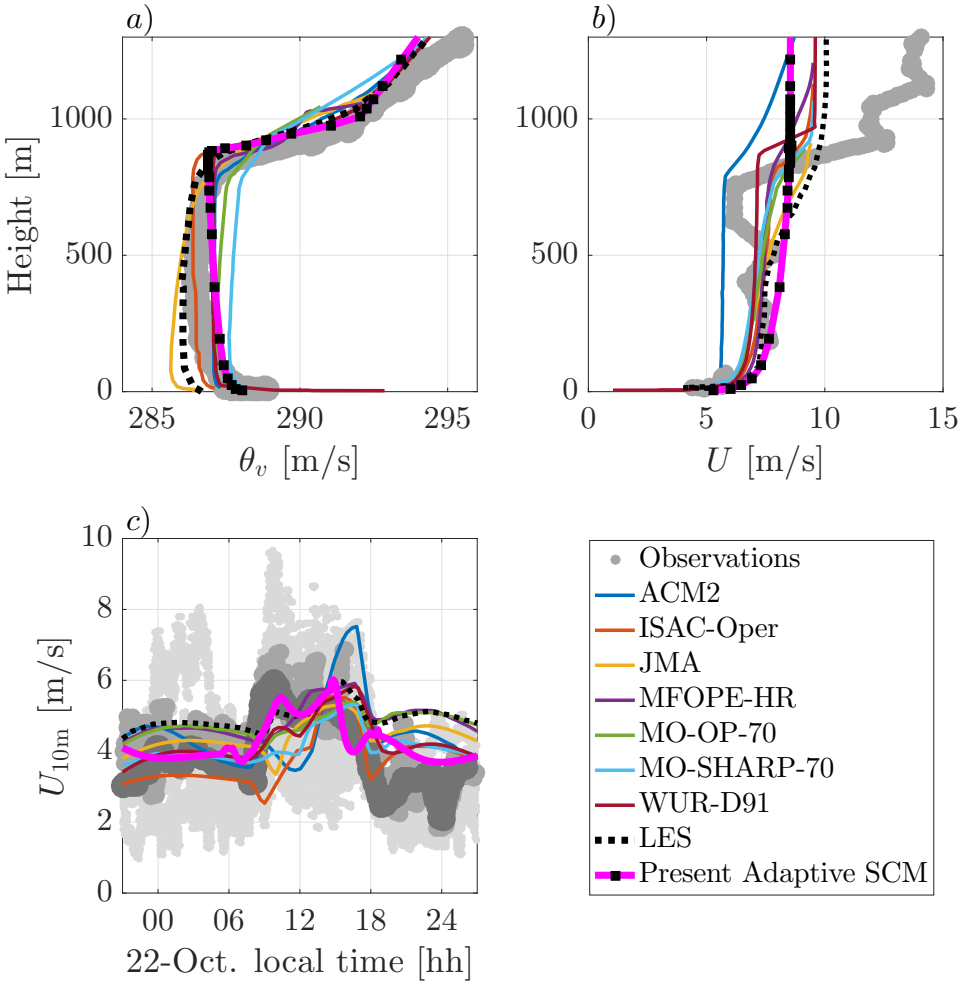

Figure 3. Intercomparison of the results obtained with the adaptive-grid SCM and the participating models in the work of (Svensson et al., 2011) for the vertical profiles of (a) the virtual potential temperature and (b) the wind-speed magnitude. Lower panel: (c) the evolution of the 10-meter wind speed (U_{10m}) on the 22-th of October. For the used model abbreviations in the legend, see Svensson et al. (2011).

Geosci. Model Dev. Discuss., https://doi.org/10.5194/gmd-2018-21
Manuscript under review for journal Geosci. Model Dev.
Discussion started: 29 March 2018

Geoscientific Model Development Discussions
Open Access
EGU

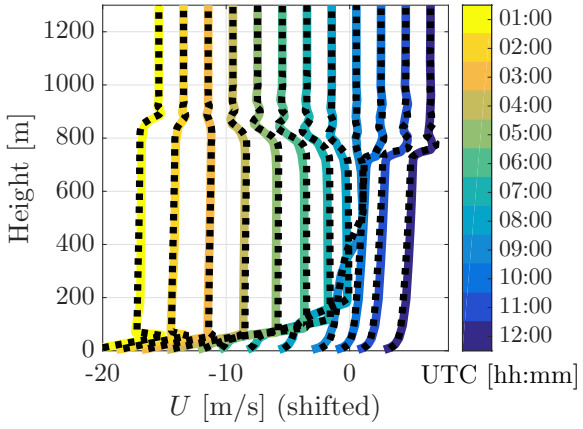

Figure 4. Vertical profiles of the wind-speed magnitude U obtained with the adaptive-grid (in colour) and the fixed equidistant-grid (dashed) SCMs. The twelve plotted profiles are obtained for the 23-th of October with an hourly interval, starting from 1:00 AM local time. Noting that the profiles are shifted in order to distinguish between the different times (with vanishing wind at the surface).

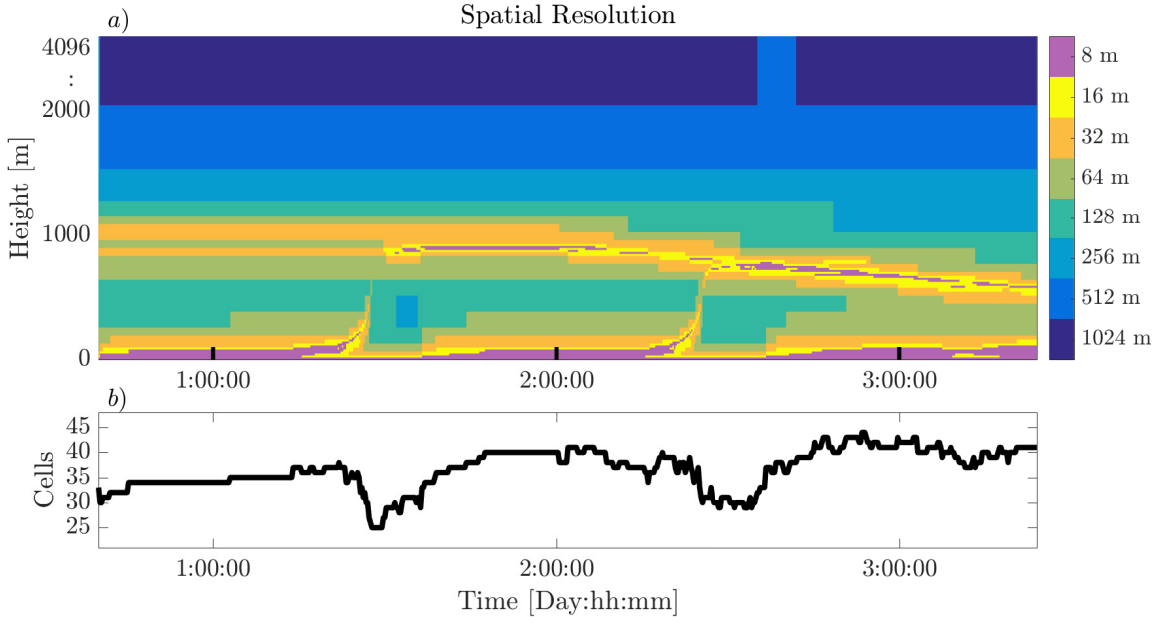

Figure 5. Evolution of (a) the vertical spatial resolution and (b) the total number of grid cells, for the GABLS2 intercomparison case.

Geosci. Model Dev. Discuss., https://doi.org/10.5194/gmd-2018-21
Manuscript under review for journal Geosci. Model Dev.
Discussion started: 29 March 2018

Geoscientific Model Development Discussions

Table 1. The exact formulation of the methods are described at the online locations of the definition files for the different cases presented in this manuscript.

Section	Case	Grid	URL: http://www.basilisk.fr...	Solver timesteps	Wall-clock time
3.1	GABLS1	Adaptive	/sandbox/Antoonvh/GABLS1.c	14404	$\approx$ 1.3 sec.
"	"	Fixed & Equidistant	/sandbox/Antoonvh/GABLS1fg.c	14404	$\approx$ 0.8 sec.
3.2	GABLS2	Adaptive	/sandbox/Antoonvh/GABLS2.c	24262	$\approx$ 9 sec.
"	"	Fixed & Equidistant	/sandbox/Antoonvh/GABLS2fg.c	33993	$\approx$ 22 sec.
Appendix	Ekman spiral	Adaptive	/sandbox/Antoonvh/ekman.c	1000 ($\times$20 runs)	$\approx$ 19 sec.
"	"	Fixed & Equidistant	/sandbox/Antoonvh/ekmanfg.c	1000 ($\times$10 runs)	$\approx$ 18 sec.

Wall-clock times are evaluated using a single core (processor model: Intel i7-6700 HQ).

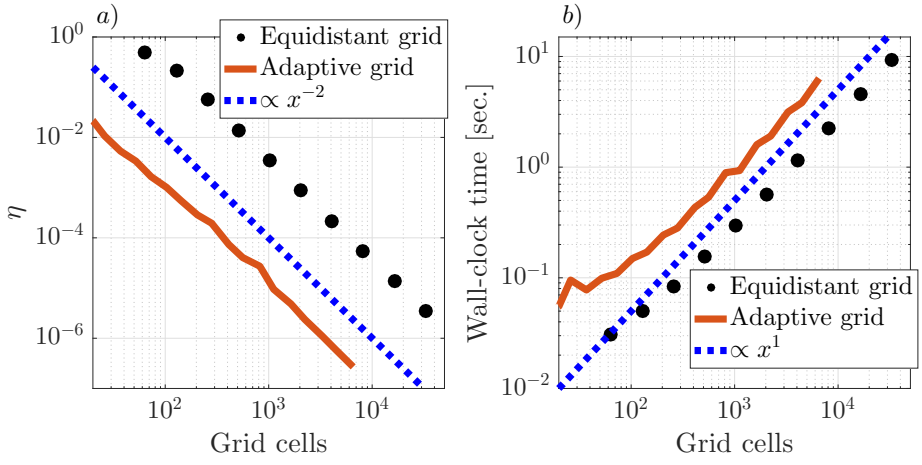

Figure A1. The scaling characteristics for the laminar-Ekman-spiral case. (a) Presents the error convergence for the equidistant-grid and adaptive-grid approach, showing that the solver is second-order accurate. The wall-clock time for the different runs is presented in (b), showing that for both of the aforementioned approaches, the required effort scales linearly with the number of grid cells.